High-spin states of the semimagic nucleus $^{151}_{69}Tm_{82}$*

X. H. Yu (余兴汉)[1,2] M. L. Liu (刘梦兰)[3,4] H. Huang (黄浩)[1,2] W. Q. Zhang (张文强)[1,2] Z. Liu (刘忠)[1,2†] M. L. Liu (柳敏良)[1,2‡] A. N. Andreyev[5] C. X. Yuan (袁岑溪)[3] P. M. Walker[6] C. Qi (亓冲)[7] J. G. Wang (王建国)[1,2] B. Ding (丁兵)[1,2] G. J. Fu (傅冠健)[8] Q. B. Zeng (曾全波)[1,2] Y. F. Wu (吴迎峰)[1,2] R. D. Page[9] B. H. Sun (孙保华)[10] C. Scholey[11] S. Eeckhaudt[11] T. Grahn[11] P. T. Greenlees[11] N. J. Thompson[6] I. G. Darby[12] A. B. Garnsworthy[13] M. B. Gómez-Hornillos[14] D. G. Jenkins[5] P. Jones[15] R. Julin[16] D. T. Joss[9] S. Ketelhut[16] M. Leino[16] M. Niikura[17] M. Nyman[18] J. Pakarinen[16] S. Pietri[19] Zs. Podolyák[6] P. Rahkila[16] J. Sarén[16] J. Uusitalo[16] S. Williams[6] H. K. Wang[20] F. S. Zhang (张丰收)[21]

[1]Institute of Modern Physics, Chinese Academy of Sciences, Lanzhou 730000, China
[2]University of Chinese Academy of Sciences, Beijing 100049, China
[3]Sino-French Institute of Nuclear Engineering and Technology, Sun Yat-sen University, Zhuhai 519082, China
[4]Center for Exotic Nuclear Studies, Institute for Basic Science, Daejeon 34126, Republic of Korea
[5]School of Physics, Engineering and Technology, University of York, York, YO10 5DD, United Kingdom
[6]Department of Physics, University of Surrey, Guildford GU2 7XH, United Kingdom
[7]KTH, Alba Nova University Center, SE-10691 Stockholm, Sweden
[8]School of Physics Science and Engineering, Tongji University, Shanghai 200092, China
[9]Department of Physics, Oliver Lodge Laboratory, University of Liverpool, Liverpool L69 7ZE, United Kingdom
[10]School of Physics, Beihang University, Beijing 100191, China
[11]Department of Physics, University of Jyväskylä, P.O. Box 35, FI-40014 Jyväskylä, Finland
[12]SUPA, School of Physics and Astronomy, University of Glasgow, Glasgow, G12 8GG, United Kingdom
[13]TRIUMF, 4004 Wesbrook Mall, Vancouver, British Columbia V6T 2A3, Canada
[14]STFC, Daresbury Laboratory, Daresbury, Warrington, WA4 4AD, United Kingdom
[15]iThemba LABS, National Research Foundation, PO Box 722, Somerset West 7129, South Africa
[16]Accelerator Laboratory, Department of Physics, University of Jyväskylä, FI-40014 Jyväskylä, Finland
[17]CNS, University of Tokyo, Tokyo 351-0100, Japan
[18]Department of Physics, University of Helsinki, FI-00014 Helsinki, Finland
[19]GSI Helmholtzzentrum für Schwerionenforschung, D-64291 Darmstadt, Germany
[20]Zhejiang Key Laboratory of Quantum State Control and Optical Field Manipulation, Department of Physics, Zhejiang Sci-Tech University, Hangzhou 310018, China
[21]The Key Laboratory of Beam Technology of Ministry of Education, College of Nuclear Science and Technology, Beijing Normal University, Beijing 100875, China

Abstract: High-spin states of the semimagic nucleus $^{151}_{69}Tm^{82}$ have been studied in the $^{96}Ru(^{58}Ni, 3p)$ reaction. The level scheme has been substantially extended to excitation energies of up to 12 MeV. More than 50 new γ-ray transitions and 40 new levels have been identified. Configuration Interaction Shell Model (CISM) calculations were performed in the full proton model space and compared with the experimental results. Four new sequences above the fully aligned $[\pi(h_{11/2})^5]_{35/2^-}$ state have been established, including proton excitations across the $Z = 64$ subshell and possible neutron excitations across the $N = 82$ shell gap.

Keywords: high-spin states, cross-shell excitation, seniority

DOI: 10.1088/1674-1137/ae84ab **CSTR:** 32044.14.ChinesePhysicsC.50094005

Received 27 April 2026; Accepted 1 July 2026; Accepted manuscript online 2 July 2026

* This work was supported by the Strategic Priority Research Program of the Chinese Academy of Sciences (XDB34000000), the National Key R&D Program of China (2018YFA0404402), the National Natural Science Foundation of China (12135004, 11635003, 12325506, 12475129), the Fundamental Research Funds for the Central Universities (22120250299, 11961141004, 11735017), and the Natural Science Foundation of Gansu Province, China (24JRRA033). A. N. Andreyev acknowledges support from the Chinese Academy of Sciences President's International Fellowship Initiative (2026PVA0208) and from STFC (ST/P004598/1, ST/V001027/1, ST/Y000242/1)

† E-mail: liuzhong@impcas.ac.cn
‡ E-mail: liuml@impcas.ac.cn

I. INTRODUCTION

Shell effects play a central role in shaping our understanding of nuclear structure. Studies of shell effects provide key tests of proton and neutron shell gaps, clarify single-particle configurations, and improve the reliability of effective nuclear interactions. One region of particular interest for such studies, both experimentally and theoretically, is around the proton subshell at Z = 64 [1] and the neutron closed shell at N = 82 [1, 2].

In the vicinity of ${}^{146}_{64}Gd_{82}$, the proton orbitals $g_{7/2}$ and $d_{5/2}$ constitute the Z = 64 subshell closure [3] and lie below the higher $0h_{11/2}$, $2s_{1/2}$, and $1d_{3/2}$ orbitals [4]. Of particular importance is the high-j orbital $0h_{11/2}$, which plays an important role in the yrast states of these nuclei. Indeed, the $\pi h^n_{11/2}$ configurations have been found to dominate high-spin levels up to the fully aligned states at 10^+, $27/2^-$, 16^+, and $35/2^-$ in ^{148}Dy, ^{149}Ho, ^{150}Er, and ^{151}Tm [5−8] with n = 2, 3, 4, and 5, respectively.

As the available angular momentum in the proton valence space becomes exhausted at higher spin and excitation energy, particle-hole (p-h) excitations across the Z = 64 proton subshell and/or the N = 82 neutron shell closure will set in and compete. Since the neutron shell gap (~4 MeV) is significantly larger than the proton subshell gap (~2 MeV) [1, 2], neutron cross-shell excitations are expected to occur at higher excitation energies than proton excitations. Indeed, such competing excitations have been identified in the N = 82 isotones ${}^{133}_{51}Sb$ [10], ${}^{134}_{52}Te$, ${}^{135}_{53}I$ [11], ${}^{136}_{54}Xe$, ${}^{137}_{55}Cs$, and ${}^{138}_{56}Ba$ [12], and tentatively assigned in ${}^{139}_{57}La$ [12] and ${}^{141}_{59}Pr$ [13].

In this work, we present new results on high-spin states of the semimagic nucleus ${}^{151}_{69}Tm_{82}$, produced via the ^{96}Ru(^{58}Ni, 3p) fusion-evaporation reaction. Its high-spin states were investigated using a selective recoil-isomer tagging (**RIT**) method [14] in combination with the prompt γ-γ coincidence technique. The experimental details are described in Sec. II, and the experimental results are presented in Sec. III. In Sec. IV, the level structures are discussed on the basis of experimental systematics in N = 82 isotones and compared with the **CISM** calculations. A summary is given in Sec. V.

II. EXPERIMENTAL DETAILS

The experiment was carried out using the gas-filled recoil separator RITU at the University of Jyväskylä. High-spin states of ^{151}Tm were populated in the ^{96}Ru(^{58}Ni, 3p) reaction. The ^{58}Ni beam was provided by the K130 cyclotron and used to bombard a self-supporting, 500 μg/cm^2 ^{96}Ru target with an isotopic enrichment of ~95% at energies of 266 MeV and 274 MeV. The beam was delivered with an average current of 3 particle nA for 110 h.

Prompt γ rays produced in the fusion-evaporation reactions were detected by the JUROGAM array [15], which consists of 43 Compton-suppressed single-crystal Ge detectors surrounding the target chamber. The detectors were positioned at angles of 72.05°, 85.84°, 94.16°, 107.94°, 133.57°, and 157.6° with respect to the beam direction. Energy and efficiency calibrations in the 0–2000 keV range were performed using ^{152}Eu and ^{133}Ba standard sources. Typical full-width-at-half-maximum (FWHM) energy resolutions for the 1408-keV line were about 3.0−3.4 keV. The in-beam data were then sorted into coincidence γ-γ matrices and a γ-γ-γ cube, and analyzed using RADWARE [16] and CERN ROOT [17]. In total, about 3 × 10^8 γ-γ-γ coincidence events were obtained.

After a time of flight of approximately 0.5 μs through the RITU separator, the evaporation residues (ERs) and their subsequent decays were detected by the GREAT spectrometer at the focal plane [18]. The ERs passed through a gas-filled multiwire proportional chamber (MWPC) and were then implanted into two 300-μm-thick, 40 mm × 60 mm double-sided silicon strip detectors (DSSSDs). A planar Ge detector was mounted behind the DSSSDs, which were surrounded by three Ge clover detectors. These detectors recorded recoil implantations, subsequent proton, α-, and β-decays, conversion electrons, X-rays, and γ rays.

III. MEASUREMENTS AND RESULTS

A. Levels below the $(27/2^-)$ isomer in ^{151}Tm

The background-subtracted spectrum of delayed γ rays within 2 μs after implantation is shown in Fig. 1. The most intense γ-ray peaks correspond to known transitions in ^{151}Tm and ^{150}Er [7, 19].

Figure 2 shows the spectrum of delayed γ rays in ^{151}Tm in coincidence with the 699- or 1478-keV transitions over the time interval $\Delta T[ER-\gamma(699,1478)]=0-2$ μs. Background spectra selected with the condition $\Delta T[ER-\gamma(699,1478)]=2-4$ μs and with a gate on the Compton background adjacent to the gating peak were subtracted. This procedure reduces contributions from γ rays associated with long-lived isomers, such as the 140-keV transition from the 30-μs isomer in ^{152}Yb [20]. Figure 2 confirms that the known isomeric γ rays of 140-, 339-, 699-, and 1478-keV are in coincidence. The time distribution $\Delta T[ER-\gamma(699,1478)]$ is shown in the inset of Fig. 2. The half-life of the isomer was measured to be 445(30) ns, in good agreement with the literature value of 466(34) ns [19].

B. High spin states above the $(27/2^-)$ isomer

RIT analysis. To investigate high-spin states in ^{151}Tm, we used the RIT technique. Figure 3 shows the background-subtracted spectrum recorded with JURO-

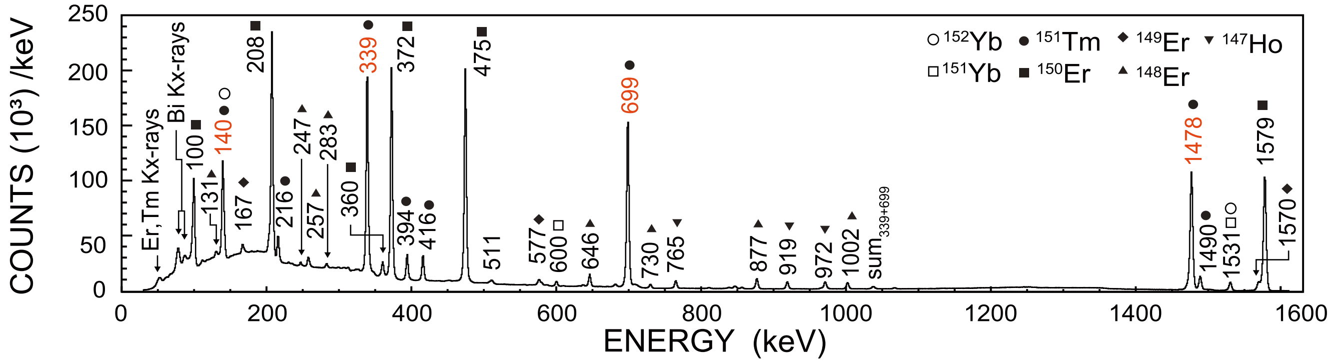

Fig. 1. (color online) The background-subtracted delayed γ-ray spectrum was recorded by the clover detectors in the GREAT spectrometer within 2 μs after ER implantation. Prominent γ rays originating from known microsecond isomers in ^{147}Ho, $^{148\text{-}150}$Er, ^{151}Tm, and $^{151\text{-}152}$Yb are labeled. The four strongest γ rays of 140, 339, 699, and 1478 keV from the known $(27/2^-)$isomer in ^{151}Tm [8−19] are highlighted in red. A background spectrum from the time interval $2 < \Delta T(ER-\gamma) < 4$ μs has been subtracted.

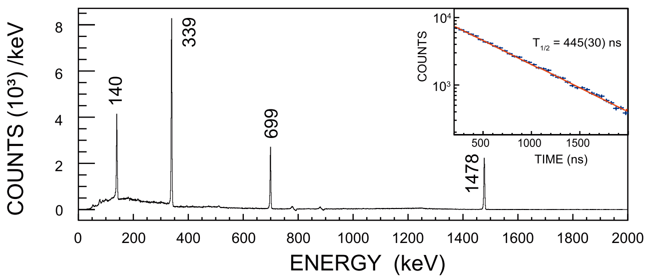

Fig. 2. (color online) The background-subtracted delayed γ-ray spectrum from γ-γ coincidences in ^{151}Tm is shown. The γ rays were gated on the 699- or 1478-keV γ rays detected with the Ge-clover detectors of the GREAT spectrometer. The inset shows the corresponding $\Delta T[ER-\gamma(699,1478)]$ time distribution.

GAM and tagged by delayed γ-ray transitions $(0 < \Delta T(ER-\gamma(699,1478)) < 2$ μs) that de-excite the $(27/2^-)$ isomer detected by the GREAT clover detectors. More than 50 new γ-ray transitions in ^{151}Tm were observed, although with reduced statistics due to losses from in-flight decay within the RITU separator.

In-beam analysis. The new transitions observed using RIT were further confirmed by γ-γ and γ-γ-γ coincidence analyses of prompt in-beam data collected with JUROGAM. Representative coincidence spectra are shown in Fig. 4, and the established level scheme is given in Fig. 5. The experimental results for these γ-ray transitions are listed in Table 1. Six level sequences, labeled Seq. 1–6, were established, of which Seq. 3–6 are new. New levels were established on the basis of the relative intensities of the γ-ray transitions and their possible multipolarities.

Sequences 1 and 2 were previously reported in Ref. [8−19] and are confirmed in this work, as shown in Figs. 4(a, e, j).

Sequence 3 has the highest intensity at high spins in ^{151}Tm and is established on top of the known 1246-keV transition, which feeds the 4613-keV level of Seq. 2. Representative coincidence spectra for Seq. 3 are shown in Figs. 4(d, h).

Three new transitions at 1872-, 1855-, and 1835-keV

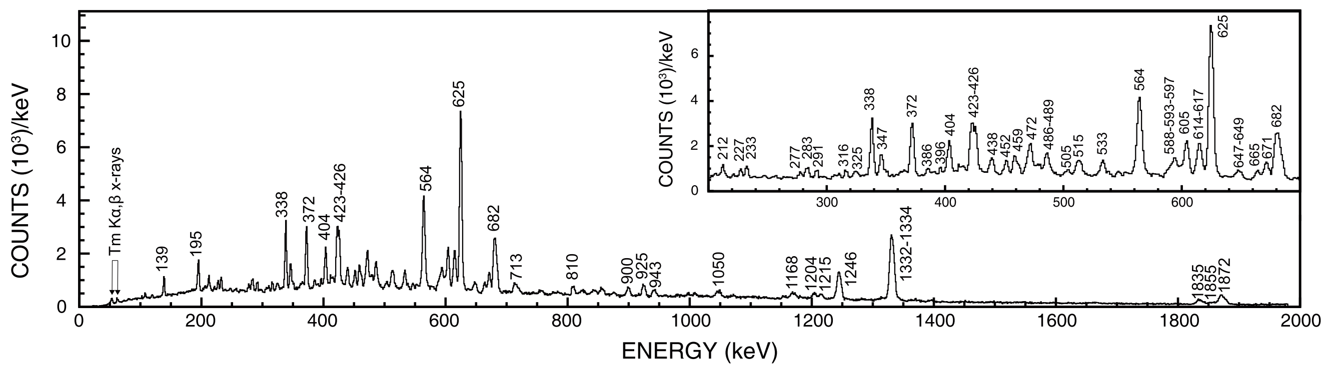

Fig. 3. The background-subtracted RIT spectrum of ^{151}Tm was measured with the JUROGAM detectors using gates on delayed γ-ray transitions $(0 < \Delta T[ER-\gamma(699,1478)] < 2$ μs) following the 0.445 μs isomer and detected with the Ge-clover detectors of GREAT. Most γ-ray peaks are newly observed in ^{151}Tm. The background spectrum was subtracted using gates on the nearby Compton background and the $2 < \Delta T[ER-\gamma(699,1478)] < 4$ μs interval. The inset shows an expanded view of the 200−700 keV region.

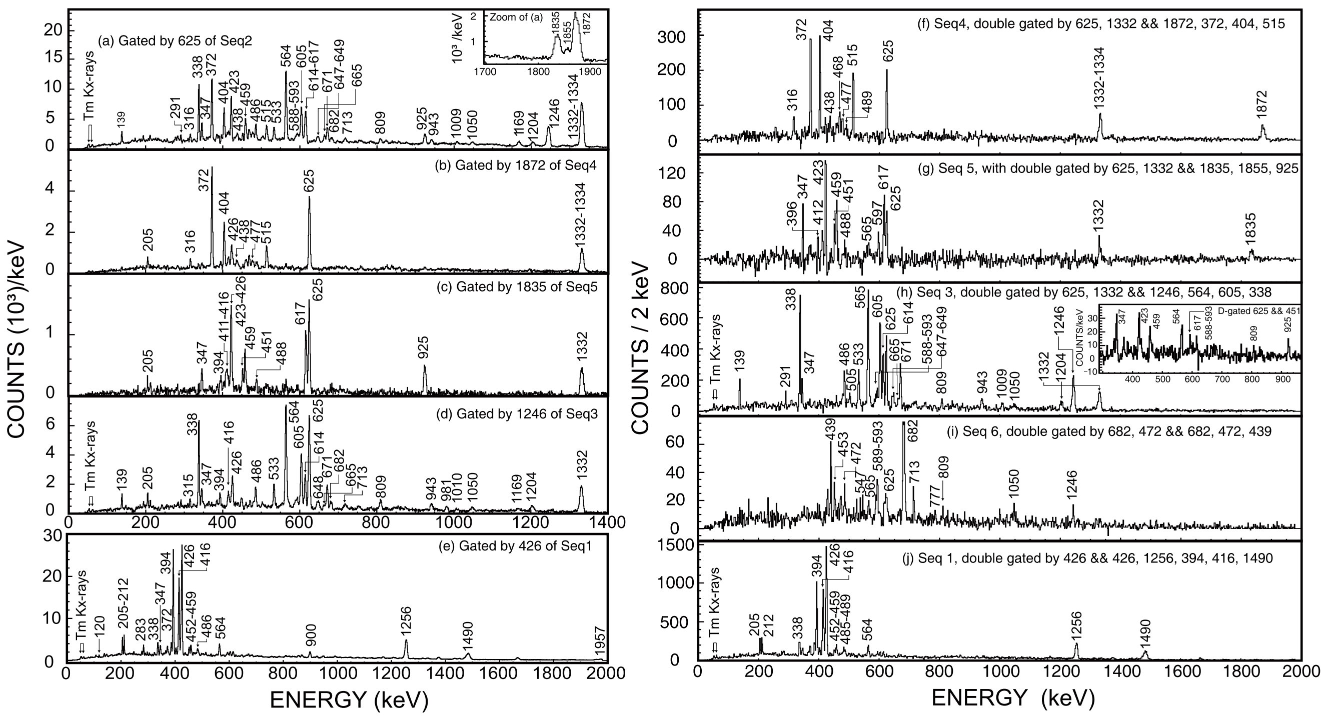

Fig. 4. Single-gated spectra from γ-γ coincidences (a)–(e) and double-gated spectra from γ-γ-γ coincidences (f)–(j), measured using only JUROGAM. Most of the peaks are new transitions in ^{151}Tm. The gating conditions are indicated, and the background was subtracted by gating on the Compton background near the gating peak.

can be seen in the 625-keV gated spectrum in the inset of Fig. 4(a), but they are not mutually coincident, as shown in Figs. 4(b, c, f, g).

Based on the γ-γ and γ-γ-γ coincidence analyses for these transitions in Figs. 4(b, c, f, g), two new sequences, labeled Seq. 4 and Seq. 5, were established. As illustrated in the inset of Fig. 4(h), the 9323-keV level in Seq. 3 also decays through the 451-keV interband transition to the 8872-keV level in Seq. 5.

Sequence 6, consisting of the 682-, 682-, 472-, 713-, and 547-keV transitions, is tentatively constructed above the known 24-ns isomer at 6909 keV [19]. Because the velocity of the ERs is approximately 1 cm/ns (corresponding to a ~500 ns flight through the RITU separator), the $\gamma-\gamma$ coincidences between transitions above and below the 24-ns isomer are not efficiently detected by the JUROGAM array (the 1050-keV transition is indicated by a dashed arrow in Fig. 5). Consequently, the transitions of Seq.6 exhibit only partial intensities in the coincidence spectrum with the 625-keV gate in Fig. 4(a), whereas the transitions above the 24-ns isomer have full intensities in the RIT spectrum (*e.g.*, the 682-keV transitions in Fig. 3).

C. Angular distributions and correlations

To investigate the multipolarities of prompt γ-ray transitions, their angular distribution (AD) and angular correlation (AC) were measured in this work. The angular distributions for the transitions [22] were extracted under RIT conditions, and representative distributions are shown in Fig. 6.

The angular distribution ratio was defined as follows:

$$R_{\rm AD} = \frac{I_\gamma(133.57^\circ \text{ or } 157.6^\circ)}{I_\gamma(85.84^\circ \text{ or } 94.16^\circ)}, \tag{1}$$

where the intensities of the γ rays (I_γ) were obtained using isomer tagging, sorted into small-angle (133.57° and 157.6°) and large-angle (85.84° and 94.16°) spectra, and normalized to the respective efficiencies of the two detector groups.

On the basis of strong transitions with known multipolarities in ^{148}Er [23], ^{150}Er [7] and ^{151}Tm [19], typical $R_{\rm AD}$ values for dipole and stretched quadrupole transitions in this work are found to be ~0.7 and ~1.24, respectively. These values were used as references for other γ rays (*i.e.*, the dashed line in Fig. 7).

We note that, because of unresolved peaks (*e.g.*, the 614- and 617-keV peaks) or low intensities (*e.g.*, transitions in Seq. 1) in the RIT spectrum, extracting R_{AD} values for such transitions is impractical.

Therefore, an alternative method based on two-point angular-correlation (anisotropy) ratios [24], denoted as R_{AC}, was used.

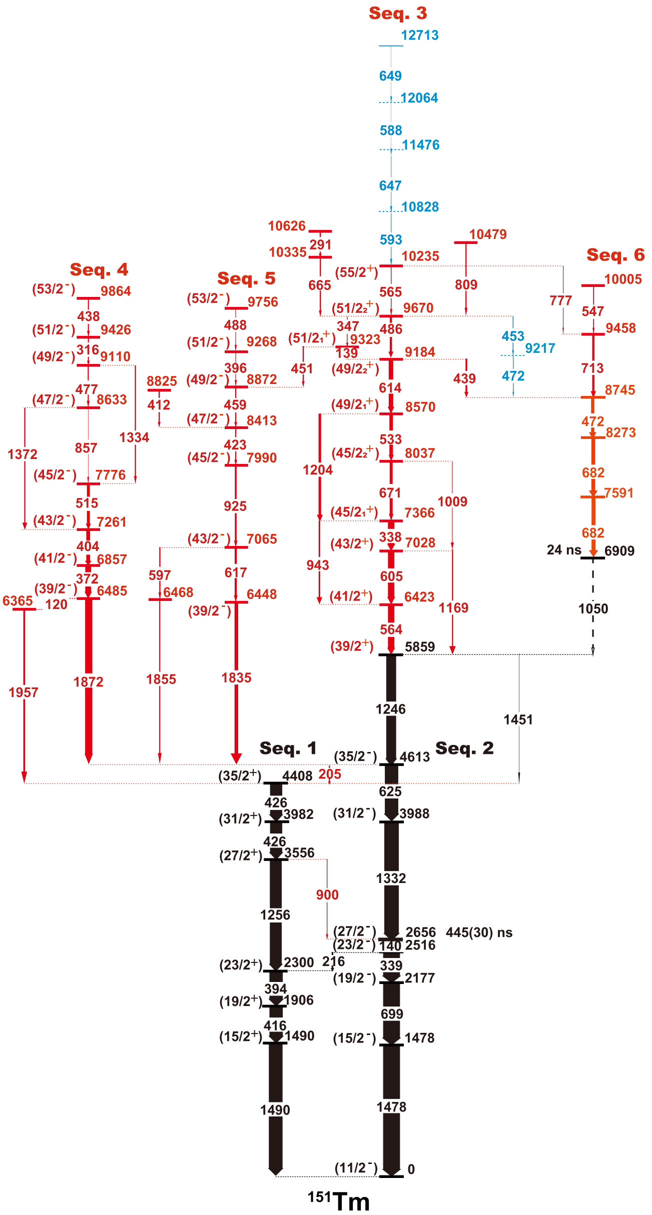

Fig. 5. (color online) Level scheme of ^{151}Tm. New transitions established in this work are shown in red or blue. The ordering of the γ rays shown in blue cannot be determined unambiguously because of limited statistics or their similar energies.

$$R_{AC} = \frac{I_\gamma(\text{at } 133.57^\circ \text{ or } 157.6^\circ, \text{gated on all angles})}{I_\gamma(\text{at } 85.84^\circ \text{ or } 94.16^\circ, \text{gated on all angles})}, \quad (2)$$

where the I_γ values were extracted from two asymmetric γ-γ coincidence matrices, with γ rays measured by Ge detectors at 133.57° or 157.6° and 85.84° or 94.16° on one axis and by all detectors on the other.

Typical R_{AC} values for known dipole and stretched quadrupole transitions in this work were ~0.7 and ~1.28, respectively. The corresponding results are shown in Table 1 and Fig. 7. Although the $R_{AD,AC}$ values for quadrupole transitions were distinct, those for E1 and M1/E2 transitions could not be distinguished. Therefore, the multipolarity assignments are guided by the theoretical interpretation in Section IV.

IV. SHELL-MODEL CALCULATIONS AND DISCUSSION

To interpret the level structure of ${}^{151}_{69}Tm_{82}$, configuration-interaction shell-model (CISM) calculations [25, 26] were performed. As shown in Fig. 8, we considered five proton orbitals between $Z = 50$ and 82, collectively denoted as $gdsh$ $(0g_{7/2}, 1d_{5/2}, 0h_{11/2}, 2s_{1/2}, 1d_{3/2})$. Owing to limitations in computational resources, the number of protons allowed to be excited across the $Z = 64$ subshell was restricted to four (denoted as $\pi(p-h)$). The neutron model space was limited to neutron orbitals below $N = 82$ (*i.e.*, without neutron excitation across the N = 82 shell gap).

In the present work, the effective Hamiltonian [26] was constructed using the monopole-based universal interaction V_{MU} [27] together with the M3Y-type spin-orbit interaction [28] (V_{MU}+LS). To reflect the experimentally observed changes in the SPEs in the range of $Z = 50-70$, the SPEs of the corresponding proton $0h_{11/2}$, $2s_{1/2}$, and $1d_{3/2}$ orbitals were lowered by 300 keV. The present calculations were performed using the code KSHELL [29]. The comparison between the experimental levels and calculated excitation energies is presented in Section A, while the orbital occupancy numbers are listed in Tables 2 and 3.

A. Proton excitations

SEQS. 1−2 In Seq. 2, the level sequence from $(11/2^-)_{g.s.}$ to $(35/2^-)$ exhibits a typical seniority pattern of the valence proton $\pi(h_{11/2})^5$ configuration [30, 31]. These states can be described by seniority quantum numbers v = 1, 3, 5, which represent the number of unpaired protons in the single-j orbital $0h_{11/2}$. This seniority pattern of Seq. 2 was well reproduced in the low-lying states of ^{150}Er, ^{151}Tm, and ^{152}Yb [30]. As shown in Fig. 9, the single-j shell model calculations agree with the experimental levels of Seq. 2 within a 500-keV deviation. When the mixing components of pair scattering and proton $p-h$ excitations across the $Z = 64$ subshell are considered, the differences between the experimental results and CISM calculations are less than 200 keV.

In Seq. 1, the positive-parity level sequence from $(15/2^+)$ to $(35/2^+)$ has $\pi d_{3/2} \otimes \pi[(h_{11/2})^4_{v=2,4}]_{6^+,8^+,10^+,12^+,14^+,16^+}$ configurations. As shown in Fig. 9, the CISM calculations are roughly 100–300 keV higher than the observed levels from $(23/2^+)$ to $(35/2^+)$, but show a significant deviation (~0.7 MeV) for the $(15/2^+)$ state due to the collective octupole nature of the 3^- core state in ^{150}Er [7].

Table 1. γ-ray energies E_γ, relative intensities I_γ, initial-to-final level energies $E_i \rightarrow E_f$, angular correlation (anisotropy) ratios R_{AC}, angular distribution ratios R_{AD}, and multipolarity assignments of the transitions in ^{151}Tm. The 625- and 1332-keV transitions of Seq. 2 are shown in bold because they are used as reference transitions for $R_{AC,AD}$.

E_γ/keV*	$I_\gamma^\&$	$I_i^\pi \rightarrow I_f^\pi$	$E_i \rightarrow E_f$	R_{AC}	R_{AD}	$ML^\#$
Seq. 1						
1490	83.2(4.2)	$(15/2^+)\rightarrow(11/2^-)$	1490 → 0	1.20(0.09)		*(M2/E3)*
416	84.4(4.2)	$(19/2^+)\rightarrow(15/2^+)$	1906 → 1490	1.11(0.08)		*(E2)*
394	86.0(5.2)	$(23/2^+)\rightarrow(19/2^+)$	2300 → 1906	1.06(0.07)		*(E2)*
1256	86.1(9.5)	$(27/2^+)\rightarrow(23/2^+)$	3556 → 2300	1.22(0.10)		*(E2)*
426	92.7(6.8)	$(31/2^+)\rightarrow(27/2^+)$	3982 → 3556	1.17(0.09)		*(E2)*
426	92.7(6.8)	$(35/2^+)\rightarrow(31/2^+)$	4408 → 3982	1.17(0.09)		*(E2)*
205	6.5(0.6)	$(35/2^+)\rightarrow(35/2^-)$	4613 → 4408	0.68(0.25)		*(E1)*
900	8.2(0.9)	$(27/2^+)\rightarrow(27/2^-)$	3556 → 2656	0.87(0.18)		*(E1)*
216$^@$		$(23/2^-)\rightarrow(23/2^+)$	2516 → 2300			*(E1)*
Seq. 2						
1478$^@$		$(15/2^-)\rightarrow(11/2^-)$	1478 → 0			*(E2)*
699$^@$		$(19/2^-)\rightarrow(15/2^-)$	2177 → 1478			*(E2)*
339$^@$		$(23/2^-)\rightarrow(19/2^-)$	2516 → 2177			*(E2)*
140$^@$		$(27/2^-)\rightarrow(23/2^-)$	2656 → 2516			*E2*
1332	**96.4(8.2)**	$\mathbf{(31/2^-)\rightarrow(27/2^-)}$	**3988 → 2656**	**1.31(0.10)**		***(E2)***
625	**100.0(5.4)**	$\mathbf{(35/2^-)\rightarrow(31/2^-)}$	**4613 → 3988**	**1.28(0.12)**	**1.13(0.11)**	***(E2)***
Seq. 3						
1246	46.8(2.5)	$(39/2^+)\rightarrow(35/2^-)$	5859 → 4613	1.18(0.12)	1.17(0.24)	*(M2/E3)*
564	39.5(7.6)	$(41/2^+)\rightarrow(39/2^+)$	6423 → 5859	0.92(0.18)		*(M1/E2)*
605	34.3(1.9)	$(43/2^+)\rightarrow(41/2^+)$	7028 → 6423	0.67(0.08)	0.87(0.17)	*(M1/E2)*
338	29.0(1.5)	$(45/2^+_1)\rightarrow(43/2^+)$	7366 → 7028	0.87(0.09)	0.76(0.13)	*(M1/E2)*
671	13.4(1.3)	$(45/2^+_2)\rightarrow(45/2^+_1)$	8037 → 7366	1.25(0.23)		*(E2)*
533	9.2(1.0)	$(49/2^+_1)\rightarrow(45/2^+_2)$	8570 → 8037	1.49(0.24)		*(E2)*
614	16.1(1.0)	$(49/2^+_2)\rightarrow(49/2^+_1)$	9184 → 8570	1.41(0.21)		*(E2)*
139	6.5(0.4)	$(51/2^+_1)\rightarrow(49/2^+_2)$	9323 → 9184	0.67(0.25)	0.55(0.18)	*(M1/E2)*
347	9.7(1.3)	$(51/2^+_2)\rightarrow(51/2^+_1)$	9670 → 9323	1.36(0.18)		*(E2)*
486	10.6(1.8)	$(51/2^+_2)\rightarrow(49/2^+_2)$	9670 → 9184	0.82(0.13)		*(M1/E2)*
565	11.5(7.6)	$(55/2^+)\rightarrow(51/2^+_2)$	10235 → 9670	1.28(0.18)		*(E2)*
593	< 4		10828 → 10235			
647	< 2		11475 → 10828			
588	< 2		12063 → 11475			
649	< 2		12712 → 12063			
809	< 4		10479 → 9670			
1169	6.6(0.5)	$(43/2^+)\rightarrow(39/2^+)$	7028 → 5859	1.42(0.19)		*(E2)*
943	5.1(0.6)	$(45/2^+_1)\rightarrow(41/2^+)$	7366 → 6423	1.45(0.16)		*(E2)*
1010	3.3(0.8)	$(45/2^+_2)\rightarrow(43/2^+)$	8037 → 7028	0.61(0.31)		*(M1/E2)*
1204	10.2(0.6)	$(49/2^+_1)\rightarrow(45/2^+_1)$	8570 → 7366	1.72(0.24)		*(E2)*

Continued on next page

Table 1-continued from previous page

E_γ/keV*	$I_\gamma^{\&}$	$I_i^\pi \rightarrow I_f^\pi$	$E_i \rightarrow E_f$	R_{AC}	R_{AD}	$ML^\#$
Seq. 4						
1872	34.5(3.5)	(39/2⁻)→(35/2⁻)	6485 → 4613	1.51(0.11)	1.64(0.13)	*(E2)*
372	28.4(1.6)	(41/2⁻)→(39/2⁻)	6857 → 6485	0.65(0.07)	0.64(0.06)	*(M1/E2)*
404	18.2(1.1)	(43/2⁻)→(41/2⁻)	7261 → 6857	0.61(0.12)	0.67(0.09)	*(M1/E2)*
515	9.1(1.0)	(45/2⁻)→(43/2⁻)	7776 → 7261	0.51(0.12)		*(M1/E2)*
857	< 2	(47/2⁻)→(45/2⁻)	8633 → 7776			*(M1/E2)*
1372	3.7(0.8)	(47/2⁻)→(43/2⁻)	8633 → 7261	1.34(0.31)		*(E2)*
1334	4.6(1.4)	(49/2⁻)→(45/2⁻)	9110 → 7776			*(E2)*
477	5.9(1.0)	(49/2⁻)→(47/2⁻)	9110 → 8632	0.61(0.24)		*(M1/E2)*
316	5.5(0.5)	(51/2⁻)→(49/2⁻)	9426 → 9110	0.57(0.19)		*(M1/E2)*
438	3.6(0.7)	(53/2⁻)→(51/2⁻)	9864 → 9426	0.62(0.21)		*(M1/E2)*
1957	< 2		6365 → 4408			
120	< 2		6485 → 6365			
Seq. 5						
1835	12.3(3.5)	(39/2⁻)→(35/2⁻)	6448 → 4613	1.47(0.20)	1.44(0.35)	*(E2)*
1855	4.8 (2.2)		6468 → 4613			
617	10.3(0.8)	(43/2⁻)→(39/2⁻)	7065 → 6448	1.26(0.22)		*(E2)*
597	3.6(1.1)		7065 → 6468			
925	11.3(0.7)	(45/2⁻)→(43/2⁻)	7990 → 7065	0.60(0.19)	0.75(0.24)	*(M1/E2)*
423	9.7(1.2)	(47/2⁻)→(45/2⁻)	8413 → 7990	0.48(0.07)		*(M1/E2)*
459	7.2(0.4)	(49/2⁻)→(47/2⁻)	8872 → 8413	0.73(0.24)		*(M1/E2)*
396	2.9(0.2)	(51/2⁻)→(49/2⁻)	9268 → 8872	0.68(0.16)		*(M1/E2)*
488	2.1(0.3)	(53/2⁻)→(51/2⁻)	9756 → 9268	0.71(0.20)		*(M1/E2)*
451	5.1(0.3)	(51/2⁺)→(49/2⁻)	9323 → 8872	0.79(0.26)		*(E1)*
Seq. 6 $						
1050			6909 → 5859			
682	20.3(4.0)		7591 → 6909			
682	20.3(4.0)		8273 → 7591			
472	11.8(3.1)		8745 → 8273			
713	3.4(0.3)		9458 → 8745			
547	< 2		10005 → 9458			
472	< 2		9217 → 8745			
453	< 2		9670 → 9217			
439	5.2(1.4)		9184 → 8745			
777	< 2		10235 → 9458			

* Due to the Doppler shift and Doppler broadening of in-beam γ peaks [21], the resolution for γ-ray energies is adopted as 1 keV.
& The relative intensities are normalized to the known 625-keV transition of Seq.2 with I_γ = 100.0.
# Multipolarity assignments are based on $R_{AD,AC}$ values in Section III.C and the theoretical interpretation in Section IV.
@ The delayed γ rays below the $(27/2^-)$ isomer. Their intensities are not compared with those of prompt γ rays in the table.
$ Seq.6 is built above the known 24-ns isomer, see the text.

The transitions from $15/2^+$ to $11/2^-$ were also found in ^{147}Tb, ^{149}Ho, and ^{151}Tm [6, 19, 32]. It is well known that such collective octupole excitations are beyond the scope of shell model description. Based on the empirical shell-

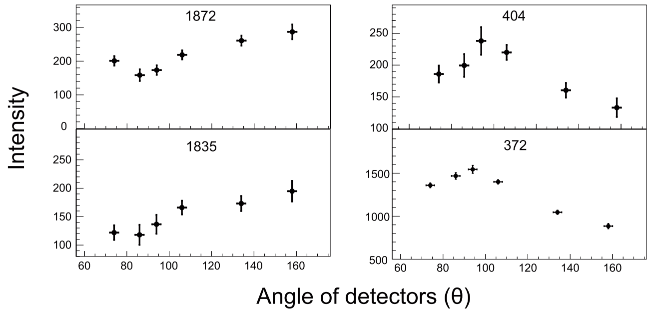

Fig. 6. Representative angular distributions of γ-ray transitions extracted from RIT. The γ-ray energies (in keV) are indicated in each panel.

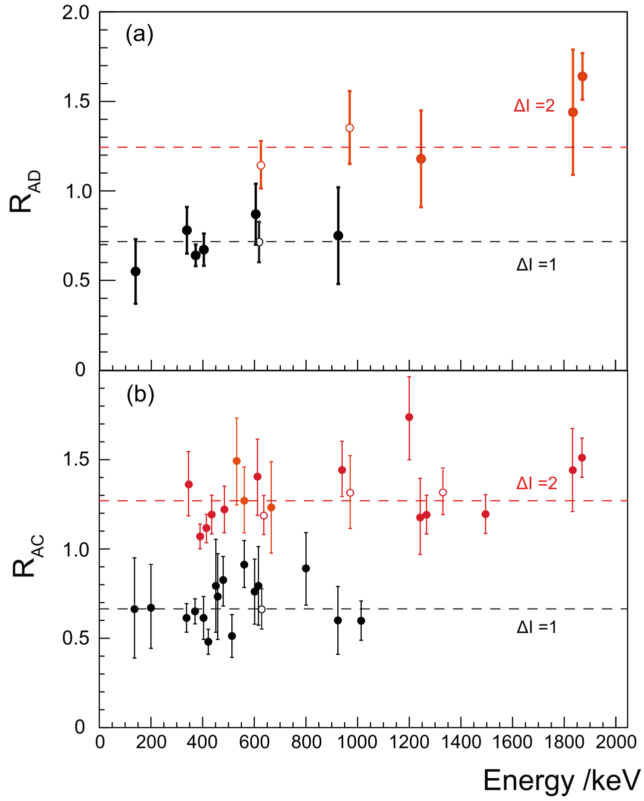

Fig. 7. (color online) The R_{AD} and R_{AC} ratios deduced in this work are shown. Reference values are indicated by open circles and horizontal dashed lines.

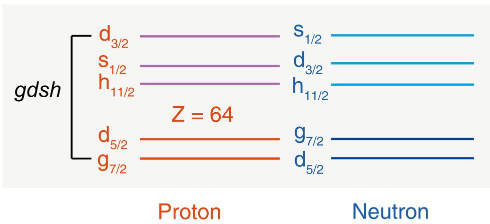

Fig. 8. (color online) Schematic diagram of proton and neutron single-particle orbits.

model description of the $[\pi h_{11/2}\otimes s_{1/2}]_{5^-}$ level in ^{150}Er [7], the considerable energy shift (~0.4 MeV) for the $(19/2^+)$ state in CISM can be explained by possible configuration mixing with $\pi s_{1/2}\otimes\pi[(h_{11/2})^4_{\nu=2}]_{10^+}$.

Table 2. The two strongest wave-function components and their partitions for the low-lying levels within CISM.

J^π	Protons per orbital					Partitions (%)
	$0g_{7/2}$	$1d_{5/2}$	$1d_{3/2}$	$2s_{1/2}$	$0h_{11/2}$	
CISM_P0						
$15/2^+$	8	6	1	0	4	31
	8	4	1	0	6	9
$19/2^+$	8	6	1	0	4	29
	8	4	1	0	6	8
$23/2^+$	8	6	1	0	4	34
	8	4	1	0	6	10
$27/2^+$	8	6	1	0	4	50
	8	4	1	0	6	11
$31/2^+$	8	6	1	0	4	55
	8	4	1	0	6	10
$35/2^+$	8	6	1	0	4	60
	8	4	1	0	6	10
CISM_N0						
$11/2^-$	8	6	2	0	3	17
	8	6	0	0	5	13
$15/2^-$	8	6	2	0	3	18
	8	6	0	0	5	14
$19/2^-$	8	6	0	0	5	19
	8	6	2	0	3	19
$23/2^-$	8	6	0	0	5	21
	8	6	2	0	3	20
$27/2^-$	8	6	0	0	5	21
	8	6	2	0	3	19
$31/2^-$	8	6	2	0	3	20
	8	6	0	0	5	17
$35/2^-$	8	6	0	0	5	40
	8	4	2	0	5	20

SEQ. 3 Since $35/2^-$ is the fully aligned state of the $[\pi(h_{11/2})^5]$ configuration, the states above it in Seq.3 likely involve p-h excitations of the $^{146}_{64}$Gd$_{82}$ core. In the $A\sim 150$ region, the $Z = 64$ proton subshell gap is approximately 2 MeV [1], while the $N = 82$ neutron shell gap is close to 4 MeV [2]. Therefore, high-spin states involving proton excitation across the $Z = 64$ subshell closure are expected to remain yrast immediately above the $[\pi(h_{11/2})^5]_{35/2^-}$ state.

The first state in Seq. 3 at 5859 keV may be of this type. It was assigned as (37/2) in previous research [19]. The spin assignment of the 5859-keV level is changed from 37/2 to 39/2 because the ADO ratio measured in the present work indicates that the 1246-keV transition has quadrupole character. According to the systematics presented in Fig. 10, it can be assigned as the fully aligned five-quasiparticle (5qp) $[\pi(h^4_{11/2}g^{-1}_{7/2})]_{39/2^+}$ state. The corresponding 4qp state with the configuration $\pi(h^3_{11/2}g^{-1}_{7/2})$ is known in ^{146}Gd (7165 keV) and ^{148}Dy (6263 keV) [7], and was newly established in ^{150}Er (6155 keV) [33].

As shown in Fig. 10, the energy differences between the 4qp and 2qp states are ~3300 keV in the neighboring even-mass $N = 82$ isotones. This energy difference can be regarded as the excitation of one proton from the $g_{7/2}$ to the $h_{11/2}$ orbital. The systematics are expected to remain robust because the Z=64 subshell and the pairing gap are stable in these isotones. For the assumed 5qp state $\pi(h^4_{11/2}g^{-1}_{7/2})_{39/2^+}$ at 5859 keV in ^{151}Tm, it may originate from the coupling of the 17⁻ state in ^{150}Er with a proton in the $h_{11/2}$ orbital when the Pauli principle is considered. The corresponding energy difference between the 5qp and 3qp states is 3203 keV, which follows the systematics and supports the above configuration assignment for the (39/2⁺) state. The 1246-keV linking transition to the (35/2⁻) state of Seq. 2 is expected to have an $M2$ character, which is also consistent with its $R_{AC,AD}$ values of ~1.2 ($\Delta I = 2$) in Table 1.

The higher-spin states from (41/2⁺) to (51/2⁺) in Seq.3 are then interpreted as 7- or 9-qp configurations involving the excitation of one or two protons from the $g_{7/2}d_{5/2}$ to the $h_{11/2}d_{3/2}s_{1/2}$ orbitals. The calculated levels with positive parity are labelled as CISM_P1 in Fig. 11. Their occupation numbers are listed in Table 3. The levels above the (39/2⁺) state are assigned as multiplets of proton p-h excitations across the Z=64 subshell closure. After angular-momentum exhaustion in the $h_{11/2}$ orbital, the other orbitals in the $gdsh$ model space have the same parity. Thus, the ΔI=1 transitions connecting these levels have $M1/E2$ character, consistent with their R_{AC} and R_{AD} values in Section III.C. The calculated excitation energies of the (39/2⁺) to (43/2⁺) states of CISM_P1 are in reasonable agreement with experiment, lying about 300 keV higher than the observed levels. They are dominated by the $\pi(1p-1h)$ excitations across the $Z = 64$ subshell with $J_{max} = (43/2^+)$. However, for the states above (43/2⁺), the deviation becomes larger. The $(45/2^+_1)$ level at 7366 keV and the $(49/2^+_1)$ level at 8570 keV are about 800 keV lower than the CISM_P1 calculations. The states above $(51/2^+_1)$ in CISM_P1 deviate substantially, lying ~1 MeV higher than the experimental levels. This discrepancy indicates that these states might be associated with the $N = 82$ neutron excitations and is discussed below together with the high-spin levels in Seq. 4−5.

SEQ. 4−5 The CISM calculations for the states from 39/2⁻ to 53/2⁻ are presented in Fig. 11. For $2p$-$2h$ excitations across the $Z = 64$ gap in ^{151}Tm, the maximum spin is

Table 3. The two dominant components of the wave functions and their partitions for the high-spin levels in CISM.

J^π	Protons per orbital					Partitions (%)
	$0g_{7/2}$	$1d_{5/2}$	$1d_{3/2}$	$2s_{1/2}$	$0h_{11/2}$	
CISM_P1						
$39/2^+$	7	6	2	0	4	44
	7	6	0	0	6	18
$41/2^+$	8	5	2	0	4	46
	8	5	0	0	6	23
$43/2^+$	7	6	2	0	4	51
	8	4	1	0	6	11
$45/2^+_1$	7	5	1	0	6	62
	7	5	3	0	4	10
$45/2^+_2$	7	5	1	0	6	48
	7	5	3	0	4	23
$49/2^+_1$	7	5	1	0	6	76
	7	4	2	0	6	6
$49/2^+_2$	7	5	1	0	6	79
	7	3	3	0	6	6
$51/2^+_1$	7	5	1	0	6	78
	7	4	2	0	6	8
$51/2^+_2$	7	4	2	0	6	80
	7	5	1	0	6	7
$53/2^+$	7	4	2	0	6	90
	7	4	1	1	6	4
$55/2^+$	7	4	2	0	6	90
	7	4	1	1	6	4
CISM_N1						
$39/2^-$	8	5	1	0	5	67
	8	4	2	0	5	7
$41/2^-$	8	5	1	0	5	77
	8	3	3	0	5	3
$43/2^-$	8	5	1	0	5	75
	8	3	3	0	5	5
$45/2^-$	7	6	1	0	5	74
	7	4	3	0	5	8
$47/2^-$	7	5	2	0	5	46
	7	5	0	0	7	27
$49/2^-$	7	5	2	0	5	84
	7	4	2	1	5	4
$51/2^-$	7	5	2	0	5	88
	7	3	2	0	7	3
$53/2^-$	7	4	1	0	7	82

Continued on next page

Table 3-continued from previous page

J^{π}	Protons per orbital					Partitions (%)
	$0g_{7/2}$	$1d_{5/2}$	$1d_{3/2}$	$2s_{1/2}$	$0h_{11/2}$	
	7	4	3	0	5	11
CISM_N2						
$39/2^-$	8	5	1	0	5	71
	8	4	2	0	5	5
$41/2^-$	8	5	1	0	5	70
	8	3	1	0	7	4
$43/2^-$	7	6	1	0	5	64
	7	5	2	0	5	10
$45/2^-$	7	5	2	0	5	62
	7	5	0	0	7	11
$47/2^-$	8	4	2	0	5	76
	7	4	1	0	7	5
$49/2^-$	7	5	2	0	5	77
	7	5	1	1	5	8
$51/2^-$	7	5	1	1	5	71
	7	4	2	1	5	7
$53/2^-$	7	4	3	0	5	70
	7	4	1	0	7	12

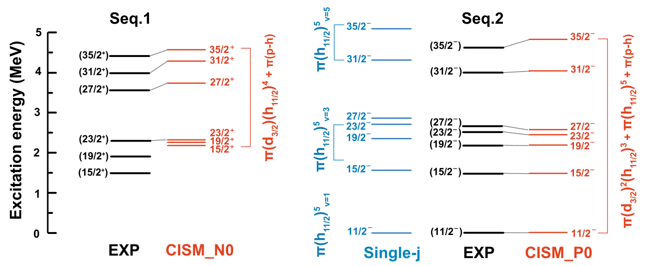

Fig. 9. (color online) A comparison is presented between the experimental level energies of Seqs. 1 and 2 and theoretical calculations for the low-lying states. The CISM calculations are indicated in red, and their occupancy numbers are listed in Table 2. The single-j shell-model calculations are taken from Ref. [30] and are indicated in blue.

51/2, corresponding to the $\pi(h_{11/2})^5\otimes\pi(d_{3/2}s_{1/2})(g_{7/2}^{-1}d_{5/2}^{-1})$ configuration.

For the states above $51/2^-$, additional proton excitations across the $Z=64$ gap would give rise to a large energy gap (~1.5 MeV) between the $53/2^-$ and $51/2^-$ states in CISM (similar to the states above $(51/2^+)$ in Seq.3), which deviates significantly from the experimental observation. Therefore, for the states above 51/2 in Seq.3-5, configurations originating from proton excitations across the $Z=64$ gap may not be yrast, as the angular momenta of protons in the $h_{11/2}$ orbital are exhausted. Thus, neutron excitations across the $N=82$ gap might be necessary, and further shell model calculations including neutron excitations are needed.

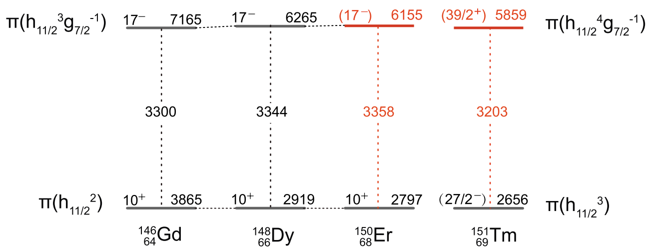

Fig. 10. (color online) Systematics of the energy differences between the fully aligned 4qp $[\pi(h_{11/2}^3g_{7/2}^{-1})_{17^-}]$ and 2qp $[\pi(h_{11/2}^2)_{10^+}]$ states in ^{146}Gd, ^{148}Dy, and ^{150}Er, and between the 5qp $[\pi(h_{11/2}^4g_{7/2}^{-1})_{39/2^+}]$ and 3qp $[\pi(h_{11/2}^3)_{27/2^-}]$ states in ^{151}Tm. The corresponding 5qp states in ^{147}Tb and ^{149}Ho have not been identified, whereas the (17^-) state in ^{150}Er [33] and the $(39/2^+)$ state in ^{151}Tm were assigned in this experiment and are marked in red.

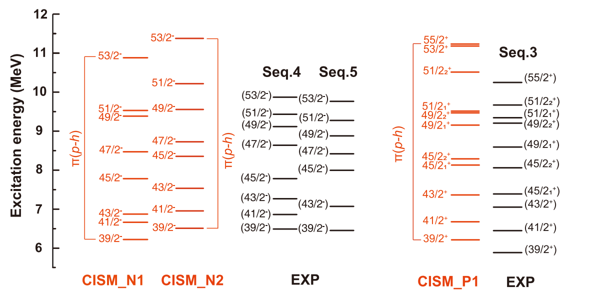

Fig. 11. (color online) CISM calculations compared with the experimental levels of Seq. 3–5 in ^{151}Tm. The calculated levels and their configurations are indicated in red.

SEQ. 6 Since the 1050-keV de-exciting transition (following the 24-ns isomer at 6909 keV) is not fully detected, the spin parities of the levels in Seq.6 are not assigned and are not compared with CISM calculations. As shown in Fig. 5, the final states at 9458 keV and 8745 keV in Seq. 6 are connected to the initial states (i.e., $(51/2_2^+)$ at 9670 keV and $(49/2_2^+)$ at 9184 keV) in Seq. 3. The final states at 9458 keV and 8745 keV in Seq. 6 may be associated with neutron core excitations, similar to their initial states in Seq. 3.

B. Possible neutron excitations across the $N=82$ shell gap

In the $N=82$ isotones with $Z<64$, excited states of the $\pi(g_{7/2}d_{5/2})^{Z-52}h_{11/2}^2$ and $\pi(g_{7/2}d_{5/2})^{Z-50}\otimes\nu(f_{7/2})(h_{11/2})^{-1}$ configurations compete [13]. For nuclei with $Z>64$, as the proton number increases from 65 to 69, the proton Fermi surface rises and the occupation number of the $\pi h_{11/2}$ orbital increases, making proton excitations from the $g_{7/2}$ and $d_{5/2}$ orbitals to the $h_{11/2}$ orbital more difficult. In addition, based on mass measurements extending to the Tm and Yb nuclei [2, 34, 35], the $N=82$ neutron shell gap shows a rapid decrease (6.5→4.0 MeV) as the proton number increases from Z = 50→58 and a gradual decline (4.0→3.6 MeV) for Z = 59→70. The observed overall reduction in the shell gap suggests that N = 82 neutron excitations are progressively facilitated in the high-spin states of ${}^{151}_{69}$Tm$_{82}$.

In Section A, the angular momenta of the valence protons become exhausted after $\pi(2p-2h)$ excitation across the $Z=64$ subshell; neutron $p-h$ excitations may then be involved in higher yrast levels with spins above (51/2). In Seqs. 3–5, the observed states above (51/2) are 1.5 MeV lower than the CISM levels calculated in the pure proton model space. Therefore, neutron excitations across the $N=82$ shell gap may be involved in these states.

V. SUMMARY

The semi-magic nucleus ^{151}Tm was produced as a residue in the fusion-evaporation reaction ^{58}Ni + ^{96}Ru at 266 and 274 MeV. A high-spin level scheme was constructed by analyzing the γ-γ coincidence data obtained with the JUROGAM array. To identify the new transitions in ^{151}Tm, we also used their coincidences with isomeric transitions detected by the focal-plane detectors of GREAT. The observed states were also compared with the results of CISM calculations. Most of the yrast states are well reproduced by these calculations. A contribution from neutron excitations across the N = 82 shell gap in the high-spin states (above 51/2) of ^{151}Tm is tentatively assigned, and further calculations of neutron excitations across the N = 82 shell gap are needed.

ACKNOWLEDGMENTS

The authors thank the JYFL staff and the ion-source crew for delivering the stable ^{58}Ni beam.

References

[1] M. Ogawa, R. Broda, K. Zell *et al.*, Phys. Rev. Lett. **41**, 289 (1978)
[2] S. Beck, B. Kootte, Dedes *et al.*, Phys. Rev. Lett. **127**, 112501 (2021)
[3] P. Mukherjee, R. Bhattacharya, and I. Mukherjee, Phys. Rev. C **24**, 1810 (1981)
[4] O. Sorlin and M.-G. Porquet, Progress in Particle and Nuclear Physics **61**, 602 (2008)
[5] P. J. Daly, P. Kleinheinz, R. Broda *et al.*, Zeitschrift für Physik A Atoms and Nuclei **298**, 173 (1980)
[6] J. Kownacki, C. Droste, T. Morek *et al.*, Phys. Rev. C **81**, 044305 (2010)
[7] Y. H. Chung, P. J. Daly, H. Helppi *et al.*, Phys. Rev. C **29**, 2153 (1984)
[8] H. Helppi, Y. Chung, P. Daly *et al.*, Physics Letters B **115**, 11 (1982)
[9] E. Nolte, G. Korschinek, and C. Setzensack, Zeitschrift für Physik A Hadrons and nuclei **309**, 33 (1982)
[10] W. Urban, A. Z lomaniec, G. S. Simpson *et al.*, Phys. Rev. C **79**, 037304 (2009)
[11] C. T. Zhang, P. Bhattacharyya, P. J. Daly *et al.*, Phys. Rev. Lett. **77**, 3743 (1996)
[12] A. Astier, M.-G. Porquet, T. Venkova *et al.*, Phys. Rev. C **85**, 064316 (2012)
[13] Z. Q. Li, S. Y. Wang, L. Liu *et al.*, Phys. Rev. C **91**, 064319 (2015)
[14] C. Scholey, D. M. Cullen, E. S. Paul *et al.*, in Exotic Nuclei and Atomic Masses, edited by J. Äystö, P. Dendooven, A. Jokinen *et al.* (Berlin, Heidelberg: Springer Berlin Heidelberg, 2003), p. 494
[15] J.Simpson, Zeitschrift für Physik A Hadrons and nuclei **358**, 139 (1997)
[16] D. Radford, Nucl. Instrum. Methods Phys. Res. A **361**, 297 (1995)
[17] R. Brun and F. Rademakers, Nucl. Instrum. Methods Phys. Res. A **389**, 81 (1997)
[18] A. Andreyev, P. Butlera, R. Page *et al.*, Nucl. Instrum. Methods Phys. Res. A **533**, 422 (2004)
[19] J. H. MCNEILL, *The Proton-Rich N = 82 and N = 83 Nuclei 151Tm, 150Ho, 151Er, and 152Tm*, Ph.D. thesis (West Lafayette, Indiana: Purdue University, 1987)
[20] D. Nisius, R. V. F. Janssens, I. G. Bearden *et al.*, Phys. Rev. C **52**, 1355 (1995)
[21] J. Pakarinen, Probing non-yrast structures of 186Pb in a RDT measurement employing the JUROGAM array, Ph.D. thesis (Jyväskylä: University of Jyväskylä, 2005)
[22] E. Der Mateosian and A. Sunyar, Atomic Data and Nuclear Data Tables **13**, 391 (1974)
[23] H. Roth, S. Arnell, D. Foltescu *et al.*, Eur. Phys. J. A **10**, 275 (2001)
[24] C. J. Chiara, M. Devlin, E. Ideguchi *et al.*, Phys. Rev. C **75**, 054305 (2007)
[25] M. Liu and C. Yuan, International Journal of Modern Physics E **32**, 2330003 (2023)
[26] J. Chen, M. Liu, C. Yuan *et al.*, Phys. Rev. C **107**, 054306 (2023)
[27] T. Otsuka, T. Suzuki, M. Honma *et al.*, Phys. Rev. Lett. **104**, 012501 (2010)
[28] G. Bertsch, J. Borysowicz, H. McManus *et al.*, Nuclear Physics A **284**, 399 (1977)
[29] N. Shimizu, T. Mizusaki, Y. Utsuno *et al.*, Computer Physics Communications **244**, 372 (2019)
[30] R. D. Lawson, Zeitschrift für Physik A Atoms and Nuclei **303**, 51 (1981)
[31] T. Matsuzawa, H. Nakada, K. Ogawa *et al.*, Phys. Rev. C **62**, 054304 (2000)
[32] R. Collatz, P. Kleinheinz, C. Zhang *et al.*, Zeitschrift für Physik A Hadrons and nuclei **351**, 245 (1995)
[33] Y. F. Wu, X. H. Yu, M. L. Liu *et al.*, (2026), in preparation.
[34] F. Kondev, M. Wang, W. Huang *et al.*, Chinese Physics C **45**, 030001 (2021)
[35] B. Kootte, M. P. Reiter, C. Andreoiu *et al.*, Phys. Rev. C **112**, 024318 (2025)